IOP Publishing

Barocaloric Effects in the Solid-State
Materials and methods
Pol Lloveras

Chapter 4

Barocaloric effect in ferroelastic fluorides and oxyfluorides

Igor N Flerov, Evgeniy V Bogdanov and Mikhail V Gorev

4.1 Introduction

Intensively increasing attention of the scientific and engineering community is attracted by caloric effects (CEs) in solids, which are reversible changes in entropy or temperature under the action of an external field in isothermal and adiabatic conditions, respectively. It is generally recognized that one of the most promising areas for the search and development of new highly efficient methods of cooling is associated with the intensification of studies of CEs in solids undergoing phase transitions of varying physical nature [1–5]. In accordance with the nature of the external field and the conjugated order parameter, electro (ECE)-, magneto (MCE)-, baro (BCE)—and piezo (PCE)—caloric effects are distinguished. For many years, most attention was paid to the first two effects, which led, firstly, to the appearance of remarkable reviews devoted to MCE [5–11] and ECE [12, 13], and, secondly, to the development and implementation of models aimed at the promising use of caloric materials in refrigerators, heat pumps, energy collection and storage devices, medical devices [6, 14, 15].

Over the past decade, interest in BCE and PCE has grown noticeably and continues to grow due to their significant advantage over other CEs [15, 16]. Indeed, both effects are universal, since phase transitions of varying physical nature are very often accompanied by significant changes in linear or bulk deformation, which, in accordance with the Maxwell relations $(\partial S/\partial p)_T = -(\partial V/\partial T)_p$ and, assuming that the compressive stress corresponds to a negative value of σ, $(\partial S/\partial \sigma)_T = (\partial L/\partial T)_\sigma$ are the defining parameters of the baro- and piezocaloric efficiency. Moreover, a comparative analysis showed that materials demonstrating CE of a mechanical nature are the most promising for use as working bodies in refrigerators and heat pumps [16, 17].

doi:10.1088/978-0-7503-4690-0ch4

To implement significant caloric parameters, one of two ways is usually used. The first is related to the search and design of new effective caloric materials [18–24]. The second one is aimed at optimizing the properties of known materials demonstrating noteworthy CEs of varying physical nature [25–32]. In the first case, it is necessary to note the recent discovery of a giant BCE in plastic crystals [18] and perovskites with organic anions [22]. A remarkable illustration of the second approach is the study of PCE in shape memory alloys, which have been very actively carried out over the past few years [21, 27, 33–38]. However, despite the significant caloric parameters of plastic crystals and organic perovskites, the gigantic temperature hysteresis of phase transitions significantly complicates the implementation of an effective reversible cooling cycle [18, 27].

Below we provide a brief overview of extensive and intensive barocaloric parameters and coefficients in relation to the degree of structural disorder and its changes during phase transitions in some fluoro- and oxyfluorometallates containing octahedral or quasi-octahedral anionic groups.

Among substances with significant BCE, complex fluorides and oxyfluorides very often demonstrate high efficient caloric characteristics [25, 34]. These compounds have as usual a strongly disordered initial cubic or orthorhombic phase and, upon cooling, undergo single or successive order–disorder phase transitions close to the tricritical point, and accompanied by a large change in entropy. Another feature of many of these materials is complex T–p phase diagrams with triple points and phase boundaries with different signs of dT/dp, which allows one both conventional and inverse BCE to be implemented in one material in fairly narrow pressure and temperature ranges [25].

The chemical pressure associated with cation–anion substitutions also turned out to be an effective tool for varying the characteristics of phase transitions (temperature, hysteresis, entropy, deformation, sensitivity to external pressures, etc) and, as a consequence barocaloric efficiency parameters.

4.2 Preliminary estimation of barocaloric parameters

Let us consider how some parameters of phase transitions affect the values and features of the temperature and pressure behavior of extensive, $\Delta S_{BCE}(T, p)$, and intensive, $\Delta T_{AD}(T, p)$, BCE in fluorides and oxyfluorides.

Regardless of the order of phase transitions (first or second) and the degree of proximity to the tricritical point, their main characteristics are: temperature, T_0, and its sensitivity to pressure dT_0/dp, the value and temperature dependence of entropy, $\Delta S_0(T)$, coefficient of volumetric thermal expansion of the crystal lattice, β_{Lat}, and others. For transformations of the first kind, the temperature hysteresis, δT_0, is also an important parameter.

The availability of information even on the approximate values of some of the above characteristics makes it possible to estimate the possible values of ΔS_{BCE} and ΔT_{AD} and, thus, to select the most promising materials for detailed studies.

4.2.1 Maximum possible values of BCE at phase transitions

In the case of a single phase transition of the first order, the maximum extensive BCE, ΔS_{BCE}, related only to the transformation (i.e., associated with the appearance of order parameter) is limited by entropy of the phase transition ΔS_0 [39] (figure 4.1).

The maximum value of intensive BCE, $\Delta T_{AD} = -T_0 \Delta S_0 / C_{Lat}$, is observed at pressure $p > p_{min}$, where C_{Lat} is the heat capacity of the crystal lattice. The minimum pressure p_{min} that produces maximum BCE values is determined by the expression

$$p_{min} = \Delta T_{AD}^{max} / (dT_0/dp) = (T_0 \Delta S_0)/(C_{Lat} dT_0/dp). \quad (4.1)$$

The maximum value of the intensive BCE ΔT_{AD}^{max} is also limited by the ΔS_0 value, and depends also on the $(\partial S_{Lat}/\partial T)_p$ derivative, i.e. on the temperature region where phase transition takes place. Figures 4.1(c) and (d) show that maximum values of ΔS_{BCE} and ΔT_{AD}, as a rule, are realized at different pressures.

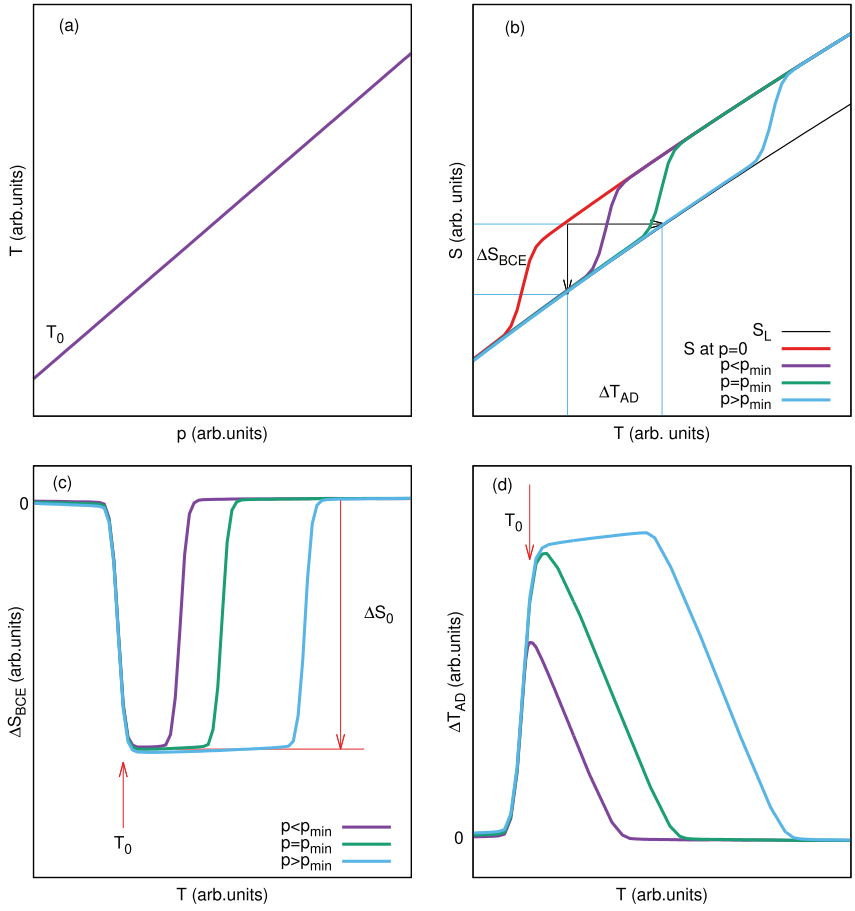

Figure 4.1. Schematic presentation of the T–p phase diagram for single phase transition (a) and related temperature dependences of extensive (b) and intensive (c) BCE at different pressures.

4.2.2 BCE and features of phase *T–p* diagrams

BCE studies are carried out on materials undergoing a single phase transition with a large change in entropy. At the same time, materials with successive phase transitions or having triple points on the *T–p* phase diagram are also of interest.

The BCE behavior of some fluorides and oxyfluorides near triple points was analyzed in [25, 40, 41]. The baric coefficients, dT/dp, for adjacent transformations in the same crystal may have the same or different signs. This means that BCE can be conventional and/or inverse in the same material at different temperatures and/or pressures. The *T–p* phase diagrams of some compounds also show triple points initiated by pressure at $p = p_{trp}$, which are associated with splitting or merging of phase boundaries with increase in pressure. So there is the possibility to change the magnitude and sign of BCE in narrow temperature and pressure ranges around the triple points.

One variant of the *T–p* phase diagram is possible in materials undergoing two successive phase transitions: with the close values of dT_1/dp and dT_2/dp characterized by the same (positive or negative) sign. In this case, BCE rises in the temperature range from $T_1(p > p^*)$ to $T_2(p = 0)$, where $p^*=(T_1 - T_2)/(dT_1/dp)$, and ΔS_{BCE}^{max} can reach a value equals to $\Delta S_1 + \Delta S_2$ and remain constant at further increase in pressure. However, the intensive BCE achieves ΔT_{AD}^{max} at higher pressure (figure 4.2).

The presence of one triple point in the *T–p* phase diagram can be associated with two variants of the BCE behavior (figure 4.3). In the first case (figure 4.3(a)), three characteristic pressure regions exist. At $T_1(p = 0) < T < T_{trp}$, increase in pressure $p \rightarrow p_{trp}$ is accompanied by an increase of extensive and intensive effects up to maximum values $\Delta S_{BCE1}^{max} = \Delta S_1$ and $\Delta T_{AD1}^{max} = -T\Delta S_1/C_{Lat}$, when $p_{min\,1} < p_{trp}$. At a pressure just above p_{trp}, the temperature region of existence of BCE associated with ΔS_1 narrows and at the same time, BCE associated with ΔS_2 appears (figure 4.3(b) and (c)).

In accordance with $dT_2/dp < 0$, at $p > p^*$ and $T < T_1(p = 0)$, the inverse BCE appears, which very quickly reaches the maximum values ΔS_{BCE} and ΔT_{AD}. Caloric effects at this pressure in the temperature ranges $T < T_1(p = 0)$ and $T > T_1(p = 0)$

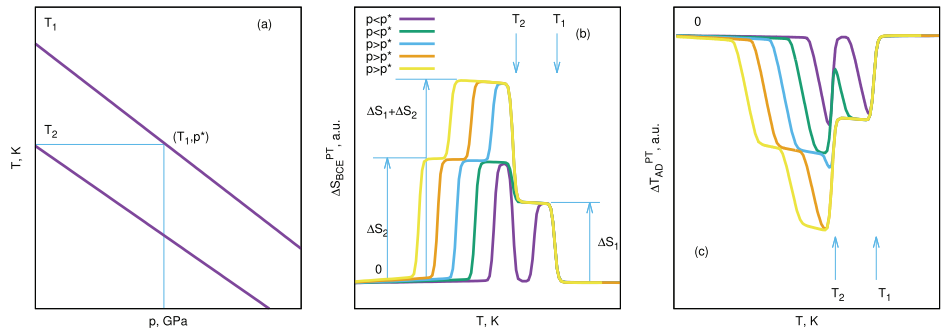

Figure 4.2. Schematic presentation of the *T–p* phase diagram for successive phase transitions (a) and related temperature dependences of extensive (b) and intensive (c) BCE at different pressures.

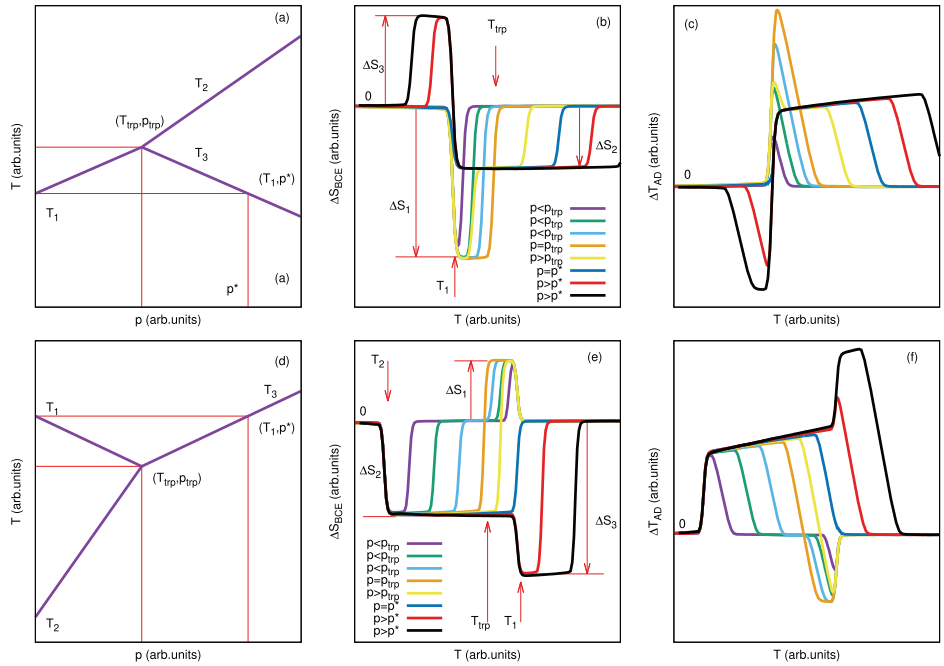

Figure 4.3. Schematic presentation of the T–p phase diagrams with triple points ((a) and (d)) and related temperature dependences of extensive ((b) and (e)) and intensive ((c) and (f)) BCE at different pressures.

depend on the parameters of phase transitions that occur at $p > p_{trp}$ and at higher pressures, $p > p_{trp} + p_{min\,2}$, $p > p_{trp} + p_{min\,3}$, they reach maximum values.

In the situation presented in figure 4.3(e) and (f), extensive and intensive BCE associated with the distinct phase transitions at $p < p_{trp}$ are observed below $T_1(p = 0)$ and above $T_2(p = 0)$. These two temperature regions expand under pressure up to the triple point, and both BCEs can achieve maximum values when p_{trp} is lower than $p_{min\,1}$ and $p_{min\,2}$. At $p > p_{trp}$, the temperature region with conventional BCE continues to expand. The range of existence of inverse BCE narrows and disappears at $p = p^*$. Above $T_1(p = 0)$, further increase in pressure leads to the appearance of BCE with the following values: $\Delta S_{BCE} = \Delta S_1 + \Delta S_2$ and $\Delta T_{AD} = -T\Delta S_{BCE}/C_{Lat}$.

The schematic phase diagrams considered above do not demonstrate all the possible variants of the dependences $T(p)$. However, their analysis is very important and informative because it allows one to see the qualitative behavior of extensive and intensive BCE in conventional and inverse variants at successive structural transformations and to carry out preliminary evaluations of the range of the p and T parameters associated with the most pronounced extensive and intensive BCE.

4.2.3 Thermal hysteresis of phase transition and reversibility of BCE

Thermal hysteresis during first-order phase transitions can prevent the system from recovering to its original state after completion of the thermodynamic cycle. Overcoming this obstacle introduces the minimum pressure threshold required to

obtain reversible BC effects, p_{rev}, which leads to excessive input work and, hence, to a subsequent decrease in performance.

Therefore, materials demonstrating transitions with small hysteresis are highly preferable. Using the known values of δT_0 and dT_0/dp, we can determine the minimum pressure to achieve reversible BCEs $p_{rev} = \delta T_0/dT_0/dp$ [18].

In the case of a positive value of dT_0/dp, endothermic transitions occur on heating or pressure reduction, while exothermic transitions occur both on cooling and on pressure increase. This means that the irreversible changes in isothermal entropy that occur when the pressure changes between $p = 0$ and a given pressure $p \neq 0$ are calculated as

$$\Delta S(T, p \to 0) = S_H(T, 0) - S_H(T, p) \tag{4.2}$$

$$\Delta S(T, 0 \to p) = S_C(T, p) - S_C(T, 0) \tag{4.3}$$

$$\Delta T(T_S, p \to 0) = T(S_H, 0) - T_S(S_H, p) \tag{4.4}$$

$$\Delta T(T_S, 0 \to p) = T(S_C, p) - T_S(S_C, 0), \tag{4.5}$$

where S_H, S_C—entropy in heating and cooling processes at constant pressure, T_S—starting temperature of process.

4.3 Experimental determination of barocaloric effect

In contrast to MCE and ECE, direct measurements of the intensive and extensive barocaloric effects are associated with a number of experimental difficulties.

There are various methods for measuring intensive caloric effects of different physical nature. However, the most reliable instrument for this purpose is an adiabatic calorimeter, which makes it possible to control and minimize heat exchange with the environment, providing adiabatic conditions, $S = \text{const}$. From calorimetric studies, in principle, one can also obtain information about the extensive caloric effect by measuring the heat capacity of materials as a function of temperature and the field of the corresponding nature.

Unfortunately, the adiabatic calorimeter is practically unsuitable for BCE studies, since in this case it is necessary to use a massive high-pressure chamber, the heat capacity of which is many times greater than the heat capacity of the sample under study. As a consequence, there is a significant loss in the accuracy of determining both the heat capacity and entropy of the sample, which makes the determination of $\Delta T_{AD}(p)$ and $\Delta S_{BCE}(p)$ practically impossible. Measurements of entropy and its changes under pressure by the DSC method, as a rule, are carried out at sufficiently low pressures and in the absence of the condition $S = \text{const}$.

Alternative indirect methods based on the use of Maxwell's equations are often used to determine extensive MCE and ECE from data on the dependences of phase transition parameter (magnetization, polarization) on the temperature and the strength of the conjugate field (magnetic and electrical). For precise calculations of BCE using this strategy, it is necessary to obtain information about the equation of state (dependence of volume on temperature and the pressure), for example, by

high-pressure diffraction methods. Unfortunately, such studies also represent a complex experimental problem and have not yet been carried out for the complex fluorides and oxyfluorides under study. To determine the extensive, ΔS_{BCE}, and intensive, ΔT_{AD}, BCE in these new compounds, we used a previously developed method based on the analysis of the experimental heat capacity at $p = 0$ and the T–p phase diagram [42, 43].

Information about the dependences of the barocaloric entropy, ΔS_{BCE}, on temperature and pressure was obtained by analyzing the total entropy of crystals at $p = 0$ and $p \neq 0$ under isothermal conditions:

$$\Delta S_{BCE}(T, p) = S(T, p) - S(T, 0). \tag{4.6}$$

The baric and temperature behavior of the intensive BCE with pressure change, ΔT_{AD}, was determined using the following relations:

$$S(T + \Delta T_{AD}, p) = S(T, 0) \tag{4.7}$$

or

$$\Delta T_{AD}(T, p) = T(S, p) - T(S, 0). \tag{4.8}$$

The total entropy of solids, $S(T, p)$, can be represented as the sum of the entropy contributions of individual subsystems: the crystal lattice, $S_{Lat}(T, p)$, the anomalous component associated with phase transitions, $\Delta S_0(T, p)$, electrons, nuclear spins, etc. Since the compounds under study are characterized mainly by ionic bonds, we can assume that at rather low pressures ($p < 1$ GPa), usually used in experiments, all contributions to the entropy except $S_{Lat}(T, p)$ and $\Delta S_0(T, p)$ do not change significantly with pressure and are not considered further.

4.3.1 Entropy at $p = 0$, $S(T, 0)$

Total entropy of compounds $S(T, 0)$, as well as anomalous, $\Delta S_0(T, 0)$, and lattice, $S_{Lat}(T, 0)$, contributions were determined by analyzing experimental heat capacity data $C_p(T, 0)$, obtained at $p = 0$ using adiabatic calorimeter. Information on C_{Lat} was obtained by fitting the experimental data $C_p(T, 0)$, taken at $T < T_i$ and $T > T_i$ far from the region of the phase transitions, using combination of Debye's and Einstein's functions: $C_{Lat}(T) = A_1 D(\Theta_D/T) + A_2 E(\Theta_E/T)$. Excess heat capacity was determined as the difference $\Delta C_p(T) = C_p(T) - C_{Lat}(T)$,

$$S(T, 0) = \int [C_p(T, 0)/T]dT = S_{Lat}(T, 0) + \Delta S_0(T, 0) = \int [C_{Lat}(T, 0)/T]dT + \int [\Delta C_p(T, 0)/T]dT. \tag{4.9}$$

4.3.2 Lattice entropy change with pressure

A change in the thermal expansion of a crystal lattice under pressure can lead to a change in the total entropy of solids and, in some cases, play a significant role in the formation of the barocaloric effect. This follows from the Maxwell equation $(\partial S_{Lat}/\partial p)_T = -(\partial V_{Lat}/\partial T)_p$, which shows that the change in isothermal entropy is proportional to the volumetric thermal expansion coefficient β_{Lat},

$$\Delta S_{\mathrm{Lat}}(T, p) = -\int \partial V_{\mathrm{Lat}}/\partial T dp \approx -V_{\mathrm{m}}\beta_{\mathrm{Lat}}(T)p. \tag{4.10}$$

Here we assume that the molar volume, V_{m}, and the coefficient $\beta_{\mathrm{Lat}}(T)$ weakly depend on pressure. Thus, if both of these parameters are characterized by large values, the change in entropy under pressure can also be large, even in materials without phase transitions.

4.3.3 Anomalous entropy change with pressure

The effect of hydrostatic pressure on the behavior of anomalous entropies has not been determined experimentally. However, taking into account the results of calorimetric studies by differential thermal analysis (DTA) under pressure for a wide range of compounds [40, 43–45], it can be assumed that the phase transition entropy, ΔS_0, which consists of a temperature-dependent part and, in the case of transformations of the first order, the jump δS_0 at T_0, as well as the degree of proximity of the phase transition to the tricritical point, are practically independent of pressure.

The temperature dependence of the anomalous entropy at various pressures, $\Delta S_0(T, p)$, was determined by the shift of the function $\Delta S_0(T, 0)$ along the temperature scale in accordance with the baric coefficients of individual phase transitions dT_0/dp:

$$\Delta S_0(T, p) = \Delta S_0(T + pdT_0/dp, 0). \tag{4.11}$$

Significant changes in the remaining components of the total entropy associated with electrons, nuclear spins, etc are most likely absent in the studied ranges of pressures and temperatures. Therefore, the temperature dependences of the total entropy at different pressures were determined by summing the entropies of the lattice and the anomalous contributions:

$$S(T, p) = S_{\mathrm{Lat}}(T, 0) + \Delta S_{\mathrm{Lat}}(T, p) + \sum \Delta S_i(T, p). \tag{4.12}$$

4.3.4 Refrigerant capacity (RC) or relative cooling power (RCP)

Integral parameters are used to assess and compare the suitability of caloric materials for use as solid-state refrigerants. One of them is the refrigerant capacity (RC) or relative cooling power (RCP) [46]. These two quantities take into account the area below the peak associated with the behavior of the function $\Delta S_{\mathrm{BCE}}(T)$ at constant pressure and are defined as $\Delta S_{\max}\times$(FWHM), where FWHM is full width at half maximum. Both RC and RCP refer to the amount of heat, which can be transferred between cold and hot reservoirs in a cycle. However, these quantities do not take into account the input work required to control the cycle and therefore an additional useful parameter is the cooling performance factor CRP (coefficient of refrigeration performance), which can be roughly calculated for BCE as CRP = $(\Delta S \times \Delta T_{\mathrm{rev}})/(p\Delta V_0/2)$, where ΔT_{rev} refers to reversible adiabatic temperature changes and ΔV_0 is the change in volume during the transition [46].

It is not possible to correctly estimate the RC or RCP parameters for all compounds analyzed in this chapter, since many of them exhibit both conventional and reverse caloric effects. There is quite a lot of arbitrariness in determining the width of the peak maximum of the BCE. However, to estimate CRP values, we can use the relation:

$$\mathrm{CRP} \approx (\Delta S_{\mathrm{BCE}} \times \Delta T_{\mathrm{rev}})/(p\Delta V_0/2) \approx 2(\Delta S_{\mathrm{BCE}} \times \Delta T_{\mathrm{rev}})/(p\Delta S_0 \times dT_0/dp). \quad (4.13)$$

4.4 Barocaloric effect in some fluorides and oxyfluorides

In this section, we will consider two groups of compounds. The first group includes the compounds Rb_2KFeF_6, Rb_2KTiOF_5, and $(NH_4)_2SnF_6$, which undergo one phase transition and are characterized by different signs of the baric coefficients dT/dp and, correspondingly, conventional and reverse BCEs. Compounds of the second group, $(NH_4)_2MoO_2F_4$, $(NH_4)_2WO_2F_4$, $(NH_4)_2NbOF_5$, demonstrate successive phase transitions, for which the influence of features of the complex phase T–p diagrams on the BCE is considered.

Complex fluorides and oxyfluorides are of undoubted interest as barocaloric materials due to a large number of their remarkable properties that manifest themselves at ambient conditions. It is known that some fairly wide crystallographic families of fluorides and oxide-fluorides can significantly change the symmetry of the structure, undergoing phase transitions with temperature and/or pressure changes [47–49].

A detailed study of phase transitions makes it possible to reveal the relationship between the chemical composition, structure and physical properties, which is key knowledge in developing an approach to the targeted creation of materials with desired properties that operate under certain environmental conditions [49].

4.4.1 Structural types, phase transitions and BCE in fluorides and oxyfuorides

One of the important features of compounds containing fluorine and/or mixed fluorine–oxygen ligands combined into six-, seven-, and eight-coordinated anionic polyhedra is related to the possibility of the formation of different crystal lattice symmetries in the initial phase: cubic, orthorhombic, etc.

Fluorides with the general chemical formula AMF_3/$A_2A'MF_6$ often crystallize in cubic form with a perovskite/double perovskite structure (sp. gr. $Pm\bar{3}m$, $Z = 1$ or $Fm\bar{3}m$, $Z = 4$), formed by vertex-linked MF_6 octahedra.

The cubic symmetry of oxyfluorides $A_2A'MO_xF_{6-x}$ is due to the static/dynamic disorder of the fluorine–oxygen ligands in the anion polyhedron, and/or such a relative orientation of the six-coordinated units located next to each other, which leads to the neutralization of the dipole moments of individual pseudo-octahedra. Both types of disorder are responsible for the fact that oxyfluorides, despite polar anions, quite often retain a nonferroelectric structure even in distorted phases resulting from phase transitions.

Materials with a perovskite-like crystal lattice have considerable potential to be disordered due to their great structural flexibility [50–52].

Among the oxyfluorides, there are also compounds $A(A')MO_xF_{6-x}$ ($x = 1, 2, 3$) and $A_2MO_xF_{6-x}$ ($x = 1, 2$) containing isolated octahedra and crystallizing in a rather low local symmetry (trigonal, tetragonal, orthorhombic) [53–55]. Additional disordering of any type of structure of fluorides and oxyfluorides can be achieved by replacing the atomic cation A^+ with the NH_4^+ tetrahedral molecular cation.

The high sensitivity of complex fluorides and oxyfluorides to variations in external (temperature, pressure) and internal (size and shape of ions, cation–anion substitution) parameters makes it possible to trace the physical nature and mechanism of changes in the stability of crystallographic phases, which arise as a result of single or successive phase transitions.

Lattice distortions caused by structural transformations are often considered in terms of two limiting mechanisms, namely displacement and/or order–disorder type mechanisms, which are characterized by a rather large difference in entropy change, ΔS: $\sim 0.1R$ and $\geqslant R \ln 2$, repectively (R is the gas constant). However, among fluorides and oxyfluorides there are a number of compounds in which the mechanism of transformations can be changed using internal chemical pressure.

The structure of fluorides and oxyfluorides with isolated octahedra can be disordered due to both octahedral and/or ammonium tetrahedral sub-subsystem. Significant entropy changes and volume jumps can be observed as a result of one and/or a sequence of phase transformations.

DTA studies under pressure of a number of complex fluorides and oxyfluorides have shown that, on the one hand, the temperatures of phase transitions are shifted to different degrees, and, on the other hand, the entropy of phase transitions practically does not change with increasing pressure [40, 43, 45].

Thermodynamic parameters of the phase transitions in the compounds under study are presented in table 4.1. As can be seen, for a number of materials, large changes in the entropy, significant shifts in the transition temperature under pressure, dT_0/dp, and

Table 4.1. Structural and thermodynamic parameters of the phase transitions in fluorides and oxyfluorides.

Compound	*PT*	T_0, K	δT_0, K	dT/dp, K GPa^{-1}	ΔS_0, J kg K^{-1}	$\Delta V_0/V$, %	Reference
Rb_2KTiOF_5	$Fm\bar{3}m$–$I4/m$	215	6.1	109.6	46.0	1.2	[43, 56, 57]
$(NH_4)_2SnF_6$	$P\bar{3}m1$–$P\bar{1}$	110	0.5	−157	61.0	−1.0	[44]
Rb_2KFeF_6	$Fm\bar{3}m$–$I4/m$	198	4.6	132	41.1	1.8	[45]
$(NH_4)_2NbOF_5$	$Cmc2_1$–$C2$	258	0.6	−45	90.0	−1.1	[26, 57, 58]
	$C2$–Ia	219	1.0	−45	69.2		
$(NH_4)_2MoO_2F_4$	$Cmcm$–$Pnma$	271	0.9	96	75.9	1.8	[59, 60]
	$Pnma$–?	180		17	7.1		
$(NH_4)_2WO_2F_4$	$Cmcm$–$P\bar{1}$	201	1.4	13.4	58.0	0.3	[60]
	$P\bar{1}$–?	161		41.7	4.3		

a small temperature hysteresis, δT_0, are observed. All this makes fluorides and oxyfluorides suitable for exhibiting significant barocaloric efficiency.

4.4.2 Ordering in the octahedral subsystem

Cubic in the initial phase, Rb_2KMF_6 elpasolites with large M cations (Sc, In, Lu, rare earth elements) undergo successive ferroelastic phase transitions $Fm\bar{3}m \leftrightarrow I4/m \leftrightarrow P12_1/n1$ upon cooling [61]. The corresponding structural distortions are considered to be associated with small-angle rotations of the MF6 octahedra. It has been established that an increase in the total entropy change during phase transitions from $0.5R$ (Sc) to $1.1R$ (Ho) with an increase in the ionic radius of M atoms correlates with an increase in the degree of anharmonicity of vibrations of critical F atoms.

A decrease in the size of the M: Fe, Cr, Ga ion leads to the appearance of one pronounced ferroelastic transition of the first order, associated with both the ordering of the octahedra and the displacement of the A^+ cation, and is accompanied by a significant change in the entropy $\Delta S \approx 2R$ [61, 62].

The substitution of the anionic group MF_6^{3-} for $TiOF_5^{3-}$ led to the presence of one phase transition $Fm\bar{3}m \leftrightarrow I4/m$ in the oxyfluoride Rb_2KTiOF_5 [56]. According to structural and IR spectral studies, the cubic phase of Rb_2KTiOF_5 is disordered in the octahedral subsystem, while the tetragonal phase is completely ordered, which corresponds to the entropy change $\Delta S = 17.0$ J mol^{-1}K $^{-1} \approx 2R$.

A $_2A'MO_x$ F $_{6-x}$ compounds with linked octahedra in the structure show a significant susceptibility of transition temperatures from the $Fm\bar{3}m$ phase and a positive sign of the pressure coefficient dT/dp. The loss of stability of the cubic phase is affected by the variation of the anionic group and/or the set of cations. An increase in external pressure leads to an increase in the phase transition temperature at a rate of $dT/dp = 132$ K GPa^{-1} and $dT/dp = 110$ K GPa^{-1} in the Rb_2KFeF_6 and Rb_2KTiOF_5 compounds, respectively (figure 4.4).

4.4.2.1 BCE in Rb_2KFeF_6, Rb_2KTiOF_5

The related compounds Rb_2KFeF_6 and Rb_2KTiOF_5 undergo single phase transition of the first order from the cubic to the tetragonal phase $Fm\bar{3}m \leftrightarrow I4m$ and are characterized by a large change in entropy ΔS_0 and a significant shift in the transition temperature under pressure dT/dp. Figures 4.5 and 4.7 show the $\Delta S_{BCE}(T, p)$ and $\Delta T_{AD}(T, p)$ dependences corresponding to the processes of pressure application and removal, and figures 4.6 and 4.8 demonstrate the maximum BCE values as a function of pressure. Because of the strong first-order phase transition in Rb_2KFeF_6, the barocaloric contributions, ΔS_{BCE}^{PT} and ΔT_{AD}^{PT}, associated with the appearance/disappearance of the order parameter, reach their maximum values already at 0.1 GPa. In Rb_2KTiOF_5, this occurs at a higher pressure, 0.2 GPa, due to the closer proximity of the phase transition to the tricritical point. This feature significantly affects also the difference in the temperature behavior of the extensive and intensive BCEs in both elpasolites. The minimum pressure to achieve reversible BC effects is low, $p_{rev} \approx 0.04$–0.06 GPa.

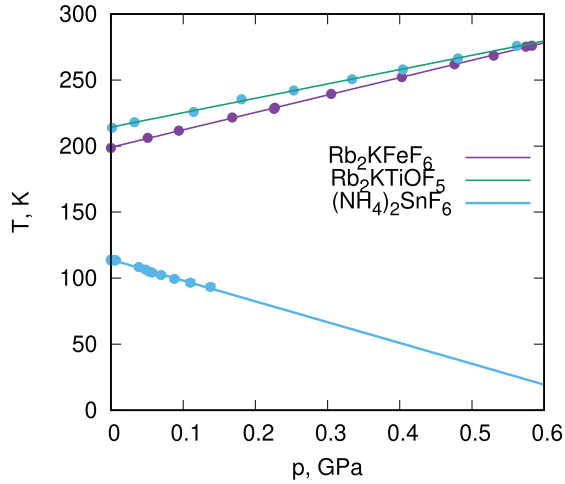

Figure 4.4. Transition temperature as a function of hydrostatic pressure for Rb_2KFeF_6, Rb_2KTiOF_5 and $(NH_4)_2SnF_6$.

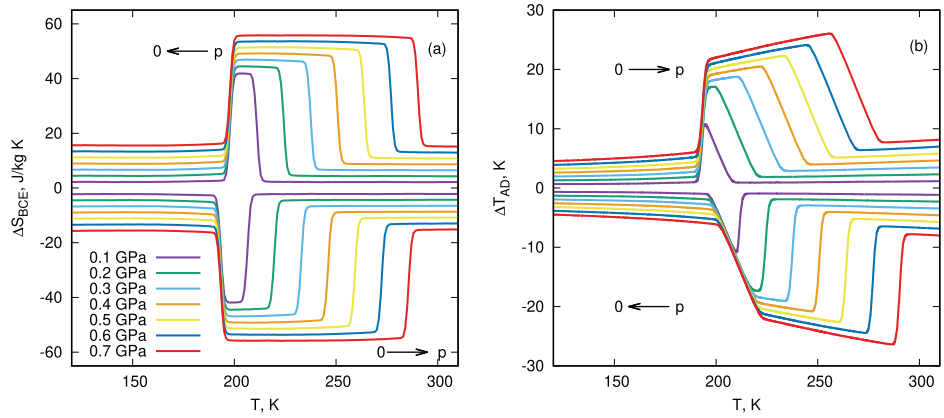

Figure 4.5. Extensive (a) and intensive (b) BCE in heating (pressure removal) and cooling (pressure application) modes in Rb_2KFeF_6.

4.4.3 Ordering of ammonium ions

At room temperature, the $(NH_4)_2SnF_6$ structure (sp. gr. $P\bar{3}m1$, $Z = 1$), which consists of isolated $[SnF_6]^{2-}$ octahedra and $[NH_4]^+$ tetrahedra, is disordered due to three equivalent orientations of two ammonium groups. The ordering of the structure occurs as a result of the phase transition $P\bar{3}m1 \leftrightarrow P\bar{1}(T_0 = 110\ \text{K})$, accompanied by a change in the entropy $\Delta S \approx R \ln 9$, corresponding to the ordering in one position of both NH_4 groups [44]. An increase in pressure leads to a decrease in the phase transition point. The boundary between $P\bar{3}m1$ and $P\bar{1}$ phases can be described by a significantly large negative baric coefficient $dT_0/dp = -157\ \text{K GPa}^{-1}$ (figure 4.4).

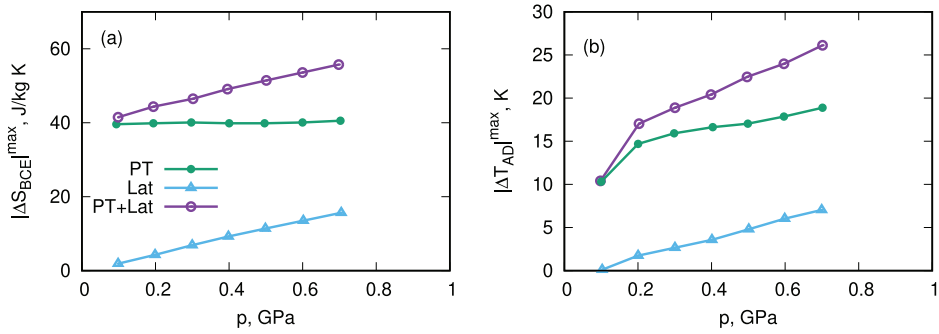

Figure 4.6. Pressure dependences of maximum values of extensive (a) and intensive (b) BCE in Rb_2KFeF_6.

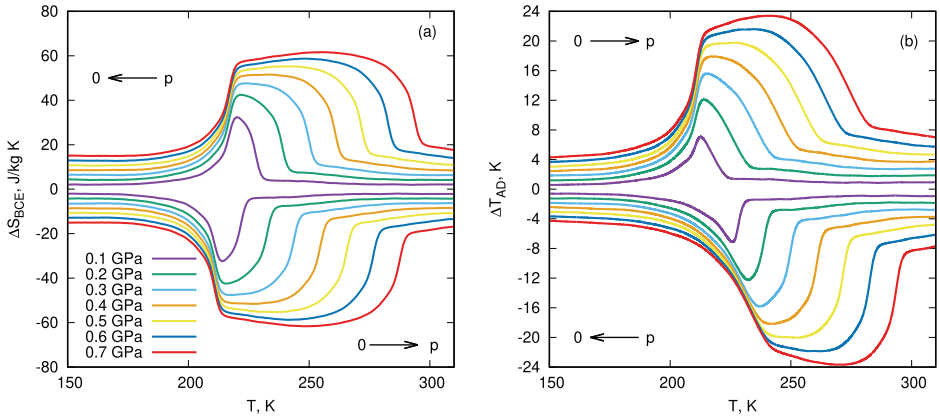

Figure 4.7. Extensive (a) and intensive (b) BCE in heating (pressure removal) and cooling (pressure application) modes in Rb_2KTiOF_5.

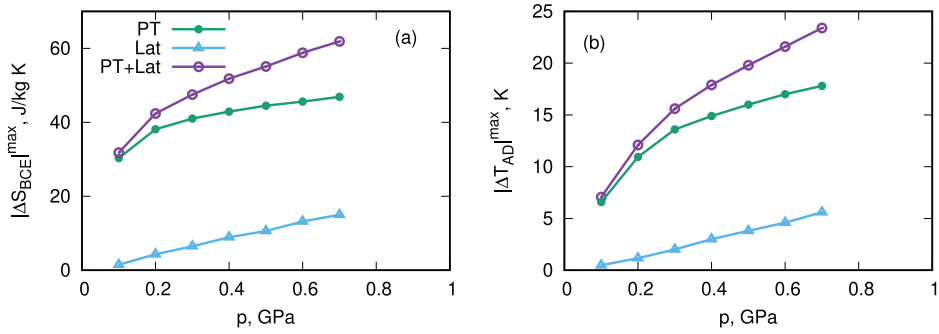

Figure 4.8. Pressure dependences of maximum values of extensive (a) and intensive (b) BCE in Rb_2KTiOF_5.

4.4.3.1 BCE in $(NH_4)_2SnF_6$

In accordance with the negative volume change near the phase transition point (figure 4.4, table 4.1), BCE in $(NH_4)_2SnF_6$ is inverse, i.e., $\Delta T_{AD} < 0$ and $\Delta S_{BCE} > 0$. A very important point is that the maximum BCE values ($\Delta S_{BCE}^{max} \approx 60$ J kg K^{-1} and

$\Delta T_{AD}^{max} \approx 11$ K) can be achieved at low pressures of 0.05–0.1 GPa (figures 4.9 and 4.10). The contributions to the extensive and intensive BCE from changes in the lattice entropy in the pressure range up to 0.2 GPa are insignificant and reach 4 J $kg^{-1}K^{-1}$ and 1 K. Figure 4.9 shows the dependences $\Delta S_{BCE}(T, p)$ and $\Delta T_{AD}(T, p)$ corresponding to the processes of applying and removing pressure for $(NH_4)_2SnF_6$. Since the phase transition in this fluoride is characterized by small value of temperature hysteresis, $\delta T \approx 0.5$ K, the minimum pressure required to achieve reversible effects is very low, $p_{rev} \approx 0.003$ GPa.

4.4.4 Structural ordering in oxyfluorides

The initial crystal structure of oxyfluorides $(NH_4)_2MO_2F_4$ (M = W, Mo) is characterized by orthorhombic symmetry (sp. gr. *Cmcm*, $Z = 4$) and consists of isolated mixed $[MO_2F_4]^{2-}$ octahedra and two nonequivalent ammonium groups [59, 63–65].

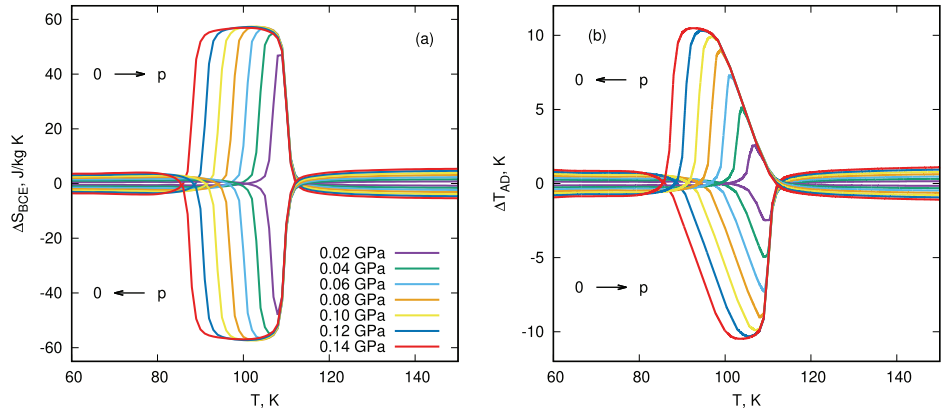

Figure 4.9. Extensive (a) and intensive (b) BCE in heating (pressure removal) and cooling (pressure application) modes in $(NH_4)_2SnF_6$.

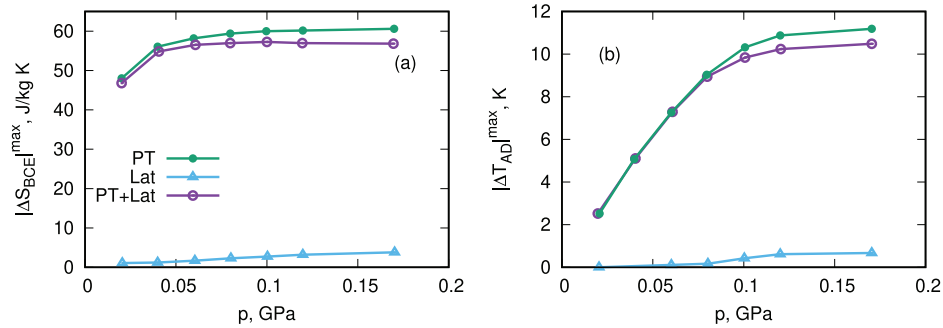

Figure 4.10. Pressure dependences of maximum values of extensive (a) and intensive (b) BCE in $(NH_4)_2SnF_6$.

The chemical pressure resulting from the substitution of the central atom: Mo (0.59 Å) → W (0.60 Å), significantly increases the stability temperature of the initial phase, and also changes the symmetry and origin of the distorted phase (antiferroelectric → ferroelastic) (table 4.1). In both compounds, the structural transformation from the initial phase *Pnma* is a first-order transition, accompanied by similar values of a significant change in entropy: W—ΔS_1=18.9 J mol^{-1}K^{-1}; Mo—ΔS_1=18.2 J mol^{-1}K^{-1}. However, the corresponding volume jumps are different: W—$\Delta V_1/V = 0.3\%$; Mo—$\Delta V_1/V = 1.8\%$. A significantly smaller change in entropy ($\Delta S_2 \approx 1.7$ J mol^{-1}K^{-1}) is observed in both oxyfluorides during the phase transition to the low-symmetry $P\bar{1}$ phase, which is associated with a slight additional displacement of structural elements.

The original orthorhombic structure is much more resistant to pressure changes in the $(NH_4)_2WO_2F_4$ ($dT_1/dp = 13$ K GPa^{-1}) than in $(NH_4)_2MoO_2F_4$ ($dT_1/dp = 93$ K GPa^{-1}) (figure 4.11). Intermediate phases in tungstate and molibdate have different symmetries, $P\bar{1}$ and *Pnma*, and are characterized by different baric coefficients $dT_2/dp = 42$ K GPa^{-1} and $dT_2/dp = 17.0$ K GPa^{-1}, respectively.

Oxyfluoride $(NH_4)_2NbOF_5$ is another outstanding example of a large structural disorder and undergoes two successive phase transitions $Cmc2_1$ ($T_1 = 258$ K) → $C2$ ($T_2 = 219$ K) →Ia [58]. In the initial phase, both octahedral and two nonequivalent tetrahedral structural units occupying 6 and 4 positions, respectively, are disordered. At T_1, the ordering is associated with a simultaneous halving of the number of orientations of each polyhedron, and at T_2, there is a complete structural ordering [66].

Both entropy values calculated within the above structural model, $\Delta S_1 = R \ln 3 + 2R \ln 2 = R \ln 12$=20.7 J (mol K)$^{-1}$ and $\Delta S_2 = R \ln 2 + 2R \ln 2 = R \ln 8 = 17.3$ J (mol K)$^{-1}$, agree well with the experimentally found entropies, $\Delta S_1 = 21.6$ J (mol K)$^{-1}$ and $\Delta S_2 = 16.6$ J (mol K)$^{-1}$.

A unique situation is typical for $(NH_4)_2NbOF_5$: an increase in pressure leads to a decrease in the temperatures of both transitions at the same rate $dT_1/dp = -45.4$ K GPa^{-1} and $dT_2/dp = -45.2$ K GPa^{-1} (figure 4.12) [26]. Thus, the intermediate phase $C2$,

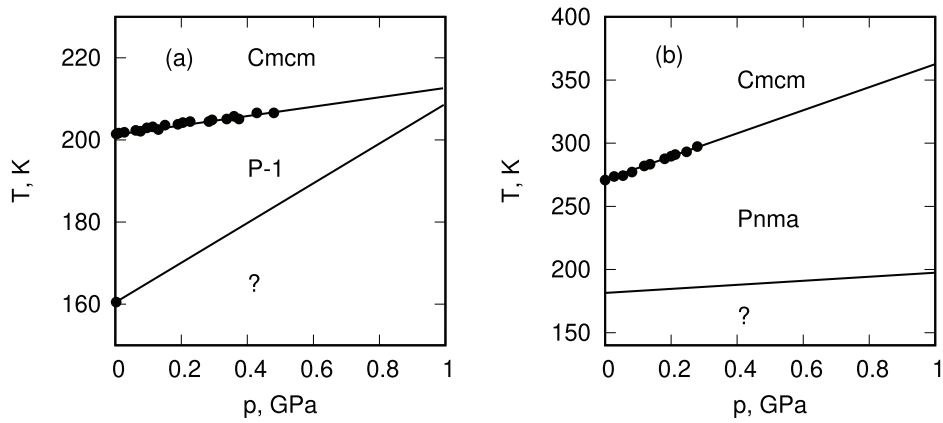

Figure 4.11. Transition temperature as a function of hydrostatic pressure for $(NH_4)_2MoO_2F_4$ (a) and $(NH_4)_2WO_2F_4$ (b).

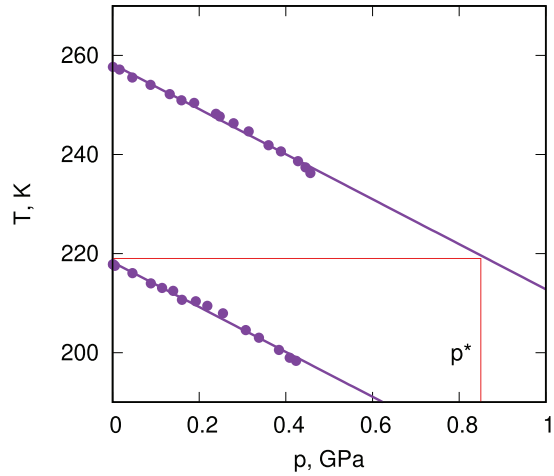

Figure 4.12. Transition temperature (peak in the calorimetric curves) as a function of hydrostatic pressure for $(NH_4)_2NbOF_5$.

for which the temperature range of existence under pressure remains unchanged, turns out to be less sensitive to external influences. In accordance with the Clausius–Clapeyron relation, the negative sign of the baric coefficients indicates a decrease in the volume of $(NH_4)_2NbOF_5$ during structural phase transitions upon heating.

4.4.4.1 BCE in $(NH_4)_2MoO_2F_4$, $(NH_4)_2WO_2F_4$

The magnitudes of the extensive and intensive BCEs in $(NH_4)_2MoO_2F_4$, $(NH_4)_2WO_2F_4$ are presented in figures 4.13 and 4.15, respectively. Despite the close values of the entropy of phase transitions at T_1, significant difference in the baric coefficients dT_1/dp leads to both a slower increase in ΔS_{BCE} and ΔT_{AD} with increasing pressure in the tungstate, and a higher value of p_{min} (figures 4.14 and 4.16). The contribution to BCE from the change in the lattice entropy with increasing pressure is significant in both oxyfluorides and, at $p \sim 1$ GPa, is comparable to the effect associated with the phase transition.

4.4.4.2 BCE in $(NH_4)_2NbOF_5$

Preliminary estimates of the BCE parameters for individual phase transitions $Cmc2_1 \leftrightarrow C2$ and $C2 \leftrightarrow Ia$ showed that, at pressure $p > p_{min} \approx 0.5$ GPa, the corresponding maximum possible values of the extensive and intensive effects ($\Delta S_{BCE}^{T1} = 90$ J (kg K)$^{-1}$, $\Delta S_{BCE}^{T2} = 69$ J (kg K)$^{-1}$ and $\Delta T_{AD}^{T1} = 22$ K, $\Delta T_{AD}^{T2} = 16$ K) can be achieved. For $p > p^* \approx (T_1 - T_2)/(dT_2/dp) \approx 0.9$ GPa, an increase in ΔS_{BCE} and ΔT_{AD} should be observed due to the summation of the effects associated with individual phase transitions (figure 4.17(a and b)). figure 4.17 shows the temperature dependences of the extensive and intensive effects before (a, b) and after (c, d) taking into account the contribution to BCE associated with the change in the entropy of the crystal lattice under pressure. As can be seen from figure 4.17(a), the extensive BCE in the region of T_2 reaches maximum possible value with increasing pressure and begins

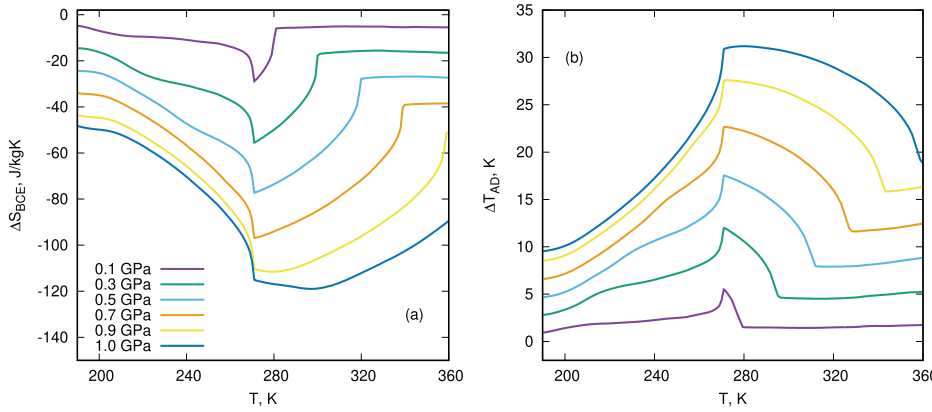

Figure 4.13. Extensive (a) and intensive (b) BCE in heating mode in $(NH_4)_2MoO_2F_4$.

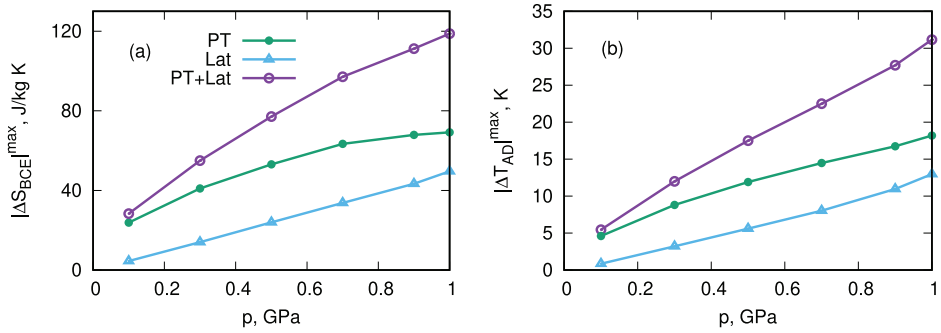

Figure 4.14. Pressure dependences of maximum values of extensive (a) and intensive (b) BCE in $(NH_4)_2MoO_2F_4$.

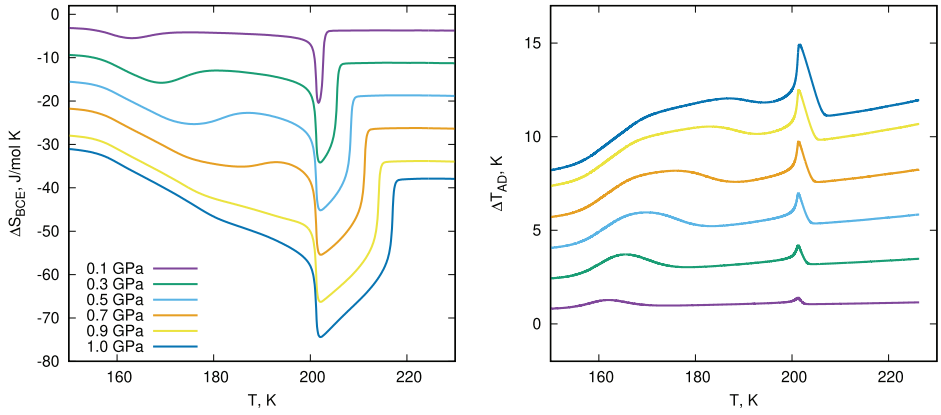

Figure 4.15. Extensive (a) and intensive (b) BCE in heating mode in $(NH_4)_2WO_2F_4$.

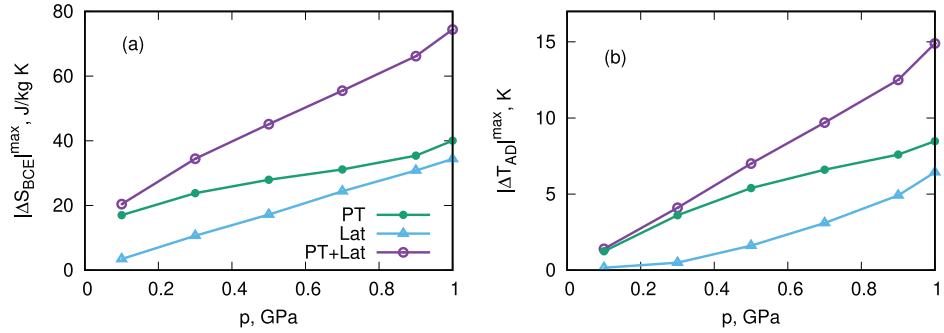

Figure 4.16. Pressure dependences of maximum values of extensive (a) and intensive (b) BCE in $(NH_4)_2WO_2F_4$.

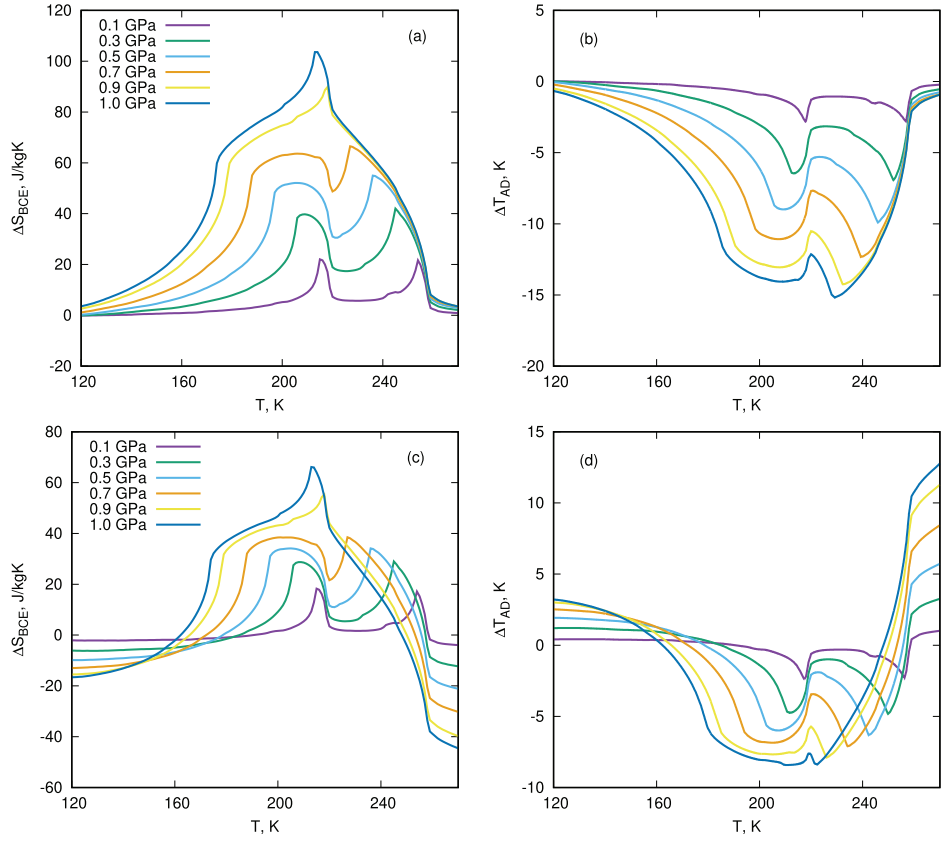

Figure 4.17. Temperature dependencies of barocaloric entropy and temperature changes in $(NH_4)_2NbOF_5$ at different hydrostatic pressures before (a, b) and after (c, d) correction for the additional lattice entropy changes with pressure.

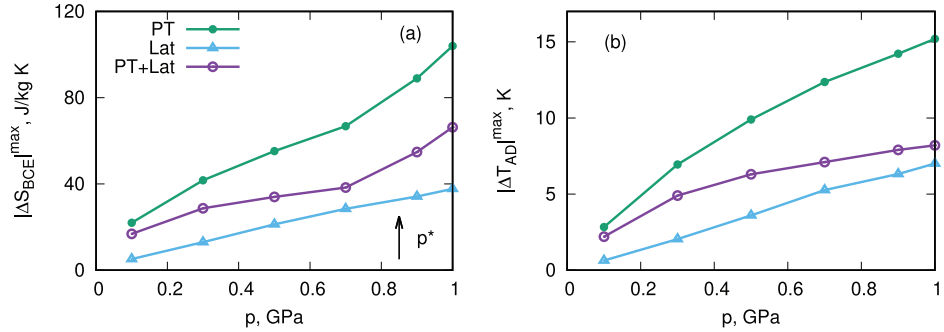

Figure 4.18. Pressure dependences of maximum values of extensive (a) and intensive (b) BCE in $(NH_4)_2NbOF_5$.

to increase again at $p > 0.7$–0.9 GPa. Due to the different signs of the thermal expansion coefficient of the crystal lattice ($\beta > 0$) and the coefficient of anomalous expansion associated with phase transitions in $(NH_4)_2NbOF_5$, the change in lattice entropy under pressure leads to a significant decrease in BCE (figure 4.17(c, d) and figure 4.18).

4.5 Conclusion

We have considered a number of fluorides and oxyfluorides that undergo individual and/or sequential phase transitions, predominantly of the order–disorder type, and demonstrate significant conventional and inverse barocaloric effects. Due to the small hysteresis of the phase transition temperature, the giant values of the isothermal entropy change and the adiabatic temperature change turned out to be reversible at sufficiently low pressures. The parameters of barocaloric effects near first-order phase transitions in some fluorides and oxyfluorides at a pressure of 0.2 GPa are presented in table 4.2.

The change in chemical pressure associated with the anion substitution and/or the central atom plays a significant role in the formation of both characteristics of the phase transitions (table 4.1) and barocaloric parameters (table 4.2).

To show the role of the cationic substation, we added to the table 4.2 oxyfluoride $(NH_4)_3TiOF_5$ not considered above, related to Rb_2KTiOF_5 and at $p = 0$ also undergoing one phase transition, characterized, on the one hand, by a very small baric coefficient, $dT/dp = 6.3$ K GPa^{-1}, but, on the other hand, a giant change in entropy $\Delta S_0 = 18.1$ J (mol K)$^{-1}$ [40, 67].

However, for $p \geqslant 0.196$ GPa, corresponding to the triple point pressure, $(NH_4)_3TiOF_5$ undergoes two successive transformations, each of which exhibits a very high sensitivity to the hydrostatic pressure: $dT_1/dp = 223$ K GPa^{-1}, $dT_2/dp = -176$ K GPa^{-1}. Due to this point, despite the division of the total entropy into two parts, $\Delta S_1 = 5.0$ J (mol K)$^{-1}$ and $\Delta S_2 = 12.8$ J (mol K)$^{-1}$, the barocaloric efficiency of ammonium oxyfluoride at T_2 turned out to be high even at a fairly low pressure, $p \approx 0.2$ GPa, and is characterized by parameters close to those found for Rb_2KTiOF_5 (table 4.2).

Table 4.2. Barocaloric parameters of some fluorides and oxyfluorides at pressure change 0.2 GPa.

Compound	T_0, K	ΔS_{BCE}^{max}, J kg K^{-1}	ΔT_{AD}^{max}, K	CRP	RC, kJ kg^{-1}	p_{rev}, GPa
Rb_2KTiOF_5	215	−40	12	0.95	0.7	0.056
$(NH_4)_2SnF_6$	110	57	−11	0.65	1.1	0.003
Rb_2KFeF_6	198	−47	17	1.47	1.2	0.035
$(NH_4)_2NbOF_5$	258 219	27	−4	0.27	0.5	0.013
$(NH_4)_2MoO_2F_4$	271 180	−45	8	0.49	1.0	0.009
$(NH_4)_2WO_2F_4$	201.5 161	−30	2.5	0.96	0.2	0.104
$(NH_4)_3TiOF_5$ [40]		−20 60	4.4 −11.5			

In this regard, in our opinion, it is promising to study solid solutions, for example, $(NH_4)_{3-x}(Rb_2K)_x$ $TiOF_5$, among which, quite likely, one can find a composition with phase transition characteristics that contribute to the implementation of optimal barocaloric parameters at even lower pressure.

In a number of fluorides and oxyfluorides under consideration, which have a triple point on the T–p phase diagram, the transition from the usual BCE to the reverse effect is observed in a narrow temperature range, in which successive structural transformations with different signs of dT/dp occur, accompanied by large changes in entropy and temperature under pressure. Materials of this kind can be considered as promising solid-state refrigerants in combined thermodynamic cycles, similar to cycles on materials with a pronounced anisotropy of the piezocaloric effect [68].

The large thermal expansion of the crystal lattice of complex oxyfluorides as well as fluorides has led in a number of crystals, characterized by $dT/dp > 0$, to an additional significant contribution comparable to the effect associated with the phase transition to the conventional BCE (figures 4.13 and 4.15). On the other hand, in the case of the inverse effect associated with $dT/dp < 0$ and, as a rule, $\beta_{Lat} > 0$, taking into account the lattice contribution reduces the total BCE. At the same time, at temperatures significantly higher than the temperature of the structural transformation in oxyfluorides, BCE may turn out to be even higher than the anomalous one observed in the region T_0 (figure 4.17).

Recently, an averaged estimate of a number of BCE parameters was carried out for some families of materials of different physical nature [34]. In comparison with these data, fluorides and oxyfluorides undergoing order–disorder transformations, accompanied by high sensitivity to hydrostatic pressure, show high barocaloric efficiency and characterized by quite satisfactory barocaloric parameters. As a result, they can be considered as promising solid-state refrigerants in the cooling devices of the future. These compounds are somewhat inferior in absolute

barocaloric characteristics to some compounds with organic cations. However, due to both relatively low pressures and a small temperature hysteresis leading to a high reversibility of the barocaloric effect, they are superior to polymers and plastic crystals.

References

[1] Mañosa L, Planes A and Acet M 2013 *J. Mater. Chem.* A **1** 4925–36
[2] Kitanovski A, Plaznik U, Tomc U and Poredoš A 2015 *Int. J. Refrig.* **57** 288–98
[3] Lorusso G *et al* 2013 *Adv. Mater.* **25** 4653–6
[4] Michaelis N, Welsch F, Kirsch S M, Schmidt M, Seelecke S and Schütze A 2019 *Int. J. Refrig.* **100** 167–74
[5] Kitanovski A 2020 *Adv. Energy Mater* **10** 1903741
[6] Gschneidner K A Jr, Pecharsky V K and Tsokol A O 2005 *Rep. Prog. Phys.* **68** 1479–539
[7] Franco V, Blázquez J, Ingale B and Conde A 2012 *Annu. Rev. Mater. Res.* **42** 305–42
[8] Smith A, Bahl C R, Bj/ork R, Engelbrecht K, Nielsen K K and Pryds N 2012 *Adv. Energy Mater.* **2** 1288–318
[9] Zhong W, Au C T and Du Y W 2013 *Chin. Phys.* B **22** 057501
[10] Planes A, Mañosa L and Acet M 2009 *J. Phys.: Condens. Matter* **21** 233201
[11] Brück E 2008 *Handbook of Magnetic Materials* (Amsterdam: Elsevier)
[12] Scott J 2011 *Annu. Rev. Mater. Res.* **41** 229–40
[13] Valant M 2012 *Prog. Mater. Sci.* **57** 980–1009
[14] Tishin A, Spichkin Y, Zverev V and Egolf P 2016 *Int. J. Refrig.* **68** 177–86
[15] Zverev V, Pyatakov A, Shtil A and Tishin A 2018 *J. Magn. Magn. Mater.* **459** 182–6
[16] Greco A, Aprea C, Maiorino A and Masselli C 2019 *AIP Conf. Proc.* **2191** 020091
[17] March 2014 Energy savings potential and RD&D opportunities for non-vapor compression HVAC technologies *Report of the U.S. Department of Energy*
[18] Aznar A, Lloveras P, Barrio M, Negrier P, Planes A, Mañosa L, Mathur N D, Moya X and Tamarit J L 2020 *J. Mater. Chem.* A **8** 639–47
[19] Bermúdez-García J M, Yáñez-Vilar S, García-Fernández A, Sánchez-Andújar M, Castro-García S, López-Beceiro J, Artiaga R, Dilshad M, Moya X and Señarís-Rodríguez M A 2018 *J. Mater. Chem.* C **6** 9867–74
[20] Bermúdez-García J M, Sánchez-Andújar M and Señarís-Rodríguez M A 2017 *J. Phys. Chem. Lett.* **8** 4419–23
[21] Li B *et al* 2019 *Nature* **567** 506–10
[22] Bermúdez-García J M, Sánchez-Andújar M, Castro-García S, López-Beceiro J, Artiaga R and Señarís-Rodríguez M A 2017 *Nat. Commun.* **8** 15715
[23] Ouyang G, Pan C, Wolf S, Mohapatra P, Takeuchi I and Cui J 2020 *Appl. Phys. Lett.* **116** 251901
[24] Zarkevich N A, Johnson D D and Pecharsky V K 2017 *J. Phys. D: Appl. Phys.* **51** 024002
[25] Gorev M, Bogdanov E and Flerov I 2017 *J. Phys. D: Appl. Phys.* **50** 384002
[26] Gorev M, Bogdanov E, Flerov I and Laptash N 2010 *J. Phys.: Condens. Matter* **22** 185901
[27] Hou H *et al* 2019 *Science* **366** 1116–21
[28] Pu Y, Zhang Q, Li R, Chen M, Du X and Zhou S 2019 *Appl. Phys. Lett.* **115** 223901
[29] Zhang G *et al* 2020 *Appl. Phys. Lett.* **116** 023902
[30] Bradeško A, Juričić D, Santo Zarnik M, Malič B, Kutnjak Z and Rojac T 2016 *Appl. Phys. Lett.* **109** 143508

[31] Hanrahan B, Easa J, Payne A, Espinal Y, Alpay S P, Kareem H, O'Brien C and Smith A 2020 *Cell Rep. Phys. Sci.* **1** 100075
[32] Liu Y, Wei J, Janolin P E, Infante I C, Kreisel J, Lou X and Dkhil B 2014 *Phys. Rev.* B **90** 104107
[33] Mañosa L and Planes A 2017 *Adv. Mater.* **29** 1603607
[34] Lloveras P and Tamarit J L 2021 *MRS Energy Sustain* **8** 3–15
[35] Cazorla C 2019 *Appl. Phys. Rev.* **6** 041316
[36] Wei Z Y, Sun W, Shen Q, Shen Y, Zhang Y F, Liu E K and Liu J 2019 *Appl. Phys. Lett.* **114** 101903
[37] Xiao F, Li Z, Chen H, Li Z, Huang K, Jin X and Fukuda T 2020 *Materialia* **9** 100547
[38] Gui W, Qu Y, Cao Y, Zhao Y, Liu C, Zhou Q, Chen J and Liu Y 2022 *J. Mater. Res. Technol.* **19** 4998–5007
[39] Pirc R, Kutnjak Z, Blinc R and Zhang Q M 2011 *Appl. Phys. Lett.* **98** 021909
[40] Gorev M, Bogdanov E and Flerov I 2017 *Scr. Mater* **139** 53–7
[41] Flerov I, Gorev M, Bogdanov E and Laptash N 2016 *Ferroelectrics* **500** 153–63
[42] Strässle T, Furrer A, Hossain Z and Geibel C 2003 *Phys. Rev.* B **67** 054407
[43] Gorev M, Flerov I, Bogdanov E, Voronov V and Laptash N 2010 *Phys. Solid State* **52** 377–83
[44] Flerov I N, Kartashev A V, Gorev M V, Bogdanov E V, Mel'nikova S V, Molokeev M S, Pogoreltsev E I and Laptash N M 2016 *J. Fluor. Chem.* **183** 1–9
[45] Flerov I, Gorev M, Tressaud A and Laptash N 2011 *Crystallogr. Rep.* **56** 9–17
[46] Aznar A, Negrier P, Planes A, Mañosa L, Stern-Taulats E, Moya X, Barrio M, Tamarit J L and Lloveras P 2021 *Appl. Mater. Today* **23** 101023
[47] Leblanc M, Maisonneuve V and Tressaud A 2015 *Chem. Rev.* **115** 1191–254
[48] Tressaud A 2010 *Functionalized Inorganic Fluorides* (Chichester: Wiley-Blackwell)
[49] Tressaud A and Poeppelmeier K (ed) 2016 *Photonic and Electronic Properties of Fluoride Materials* (Amsterdam: Elsevier)
[50] Aleksandrov K S, Anistratov A T, Beznosikov B V and Fedoseeva N V 1981 *Phase Transitions of Halide ABX_3 Compounds* (Novosibirsk: Nauka)
[51] Aleksandrov K S and Beznosikov B V 2004 *Perovskites. Present and Future* (SB RAS: Novosibirsk)
[52] Flerov I, Gorev M, Aleksandrov K, Tressaud A, Grannec J and Couzi M 1998 *Mater. Sci. Eng. R Rep.* **24** 81–151
[53] Gautier R, Gautier R, Chang K B and Poeppelmeier K R 2015 *Inorg. Chem.* **54** 1712–9
[54] Udovenko A A and Laptash N M 2008 *Acta Cryst.* **64** 645–51
[55] Udovenko A A, Vasiliev A D and Laptash N M 2010 *Acta Cryst.* **B66** 34–9
[56] Fokina V D, Flerov I N, Molokeev M S, Pogorel'tsev E I, Bogdanov E V, Krylov A S, Bovina A F, Voronov V N and Laptash N M 2008 *Phys. Solid State* **50** 2175–83
[57] Gorev M V, Bogdanov E V, Flerov I N, Voronov V N and Laptash N M 2010 *Ferroelectrics* **397** 76–80
[58] Fokina V D, Bogdanov E V, Gorev M V, Molokeev M S, Pogorel'tsev E I, Flerov I N and Laptash N M 2010 *Phys. Solid State* **52** 781–8
[59] Fokina V D, Bogdanov E V, Pogorel'tsev E I, Bondarev V S, Flerov I N and Laptash N M 2010 *Phys. Solid State* **52** 158–66
[60] Gorev M, Bogdanov E, Flerov I, Kocharova A and Laptash N 2010 *Phys. Solid State* **52** 167–75

[61] Flerov I N, Gorev M V, Tressaud A and Grannec J 1998 *Ferroelectrics* **217** 21–33
[62] Javier Zúñiga F, Tressaud A and Darriet J 2006 *J. Solid State Chem.* **179** 3607–14
[63] Flerov I N, Fokina V D, Gorev M V, Bogdanov E V, Molokeev M S, Bovina A F and Kocharova A G 2007 *Phys. Solid State* **49** 1149–56
[64] Bogdanov E V, Pogorel'tsev E I, Mel'nikova S V, Gorev M V, Flerov I N, Molokeev M S, Kartashev A V, Kocharova A G and Laptash N M 2013 *Phys. Solid State* **55** 409–18
[65] Bogdanov E V, Mel'nikova S V, Pogoreltsev E I, Molokeev M S and Flerov I N 2016 *Solid State Sci.* **61** 155–60
[66] Udovenko A A and Laptash N M 2008 *Acta Cryst.* **B64** 527–33
[67] Flerov I N, Gorev M V, Fokina V D, Bovina A F and Laptash N M 2004 *Phys. Solid State* **46** 915–21
[68] Mikhaleva E A, Gorev M V, Molokeev M S, Kartashev A V and Flerov I N 2020 *J. Alloys Compd.* **839** 155085